

A New Method for Correcting the Stress-Strain Curves after Bulging in Metals

F. Fariba^{a,*}, M. Ahmadpour^a, H. Bahrami^b

^aMechanical Engineering Department, Hamedan Branch, Islamic Azad University, Hamedan, Iran.

^bDepartment of Computer Science, South Tehran Branch, Islamic Azad University, Tehran, Iran.

Article info

Article history:

Received 2017.01.03

Received in revised form
2017.02.04

Accepted 2017.03.04

Keywords:

Stress-strain curve
Correction factor
Image processing method
Numerical simulation

Abstract

True stress-strain curve has a basic role in the analysis of deformation in theoretical plasticity and numerical simulations. Because of the triaxial state of stresses in the necking or bulging zones, in tension and the compression tests respectively, the true stress-strain curves obtained from relations are no longer valid and must be corrected. Various correction techniques have been proposed and can be found in literatures. In this study, a new semi-analytical approach for correction of the stress-strain curve in compression test for circular cross-section specimens was introduced and a relation for the correction factor was derived based on the theory of plasticity. This relation requires only a few experimental surface strain measurements which can easily be done using an image processing technique. The correction factor formula was obtained in terms of the initial radius of specimen, the bulge radius, and the surface strain on the bulge surface. The proposed approach in this study was compared with the results of the numerical simulations. Simulation was used to correct the stress-strain curve based on the optimization method with comparing the bulging profile of tested samples and ones simulated by using genetic algorithm.

Nomenclature

a_0	Initial distance between two points on the surface of the specimen	a_f	Final distance between points on the surface of the specimen
A_0	Cross sectional area of specimen in initial configuration	A_b	Cross sectional area of specimen on the buckling section
A_u^e	section area of the element in un-buckling or uniform section	A_b^e	Cross section area of the element in buckling section
CF	Correction factor	d_b	Diameter in buckling section
d_u	Diameter in the uniform section	$d\varepsilon_e$	Equivalent or effective strain
e	Engineering strain	K	Power law constant
n	The number of elements	P	Axial force
P_b^e	Axial force in the buckling end of the element "e"	P_u^e	Axial force in the uniform end of the element "e"

*Corresponding author: F. Fariba, (Assistant professor)
E-mail address: Farzad.Fariba@gmail.com

R	Curvature radius in the buckling section	r_0	Initial radius of the specimen
r_b	Radius of the buckling section	r_u	Radius of the specimen in the uniform section
r_b^e	Average radius of the element "e" in the buckling section	S	Engineering stress
t_0	Thickness of the element in the initial configuration.	t_u^e	Thickness of the elements in un-buckling end of the element "e"
t_b^e	Thickness of the elements in the buckling end of the element "e"	ε_p	Plastic strain
ε_t	True strain	ε_z	Average strain
$\varepsilon_z(r)$	Longitudinal strain function in terms of the radius	$\varepsilon_{z,s}$	Longitudinal stress on the surface of the specimen in the buckling section
σ_e	Equivalent or effective stress	σ_t	True /uncorrected stress
$\sigma_z, \sigma_r, \sigma_\theta$	Longitudinal, radial and tangential stress	σ_u	Uniform stress on un-buckling section
σ_{true}	Uncorrected true stress	$\sigma_{z,n}^e$	Longitudinal stress in the element "e" in the buckling area
z, r, θ	Longitudinal, radial and the tangential component of the coordinate		

1. Introduction

The true stress-strain curve of the metal has a significant role in the analysis of deformation in theoretical plasticity and numerical simulations. The uniaxial true stress-strain relationship is the most fundamental task before any plastic analysis that can be performed. This can define the strain hardening of a material. In metal forming industries true stress-strain curve of metals is used to design the equipment. This curve provides the yield surface that is a basic requirement in theory of plasticity. Also, true curves are used as the input of numerical modeling programs or modeling software such as ABAQUS. On the other hand, in the numerical modeling of large deformation problems, this curve represents the material model and involves constants that can influence the result of modeling. The true stress-strain curve is obtained from the engineering stress-strain curve which is computed from the load-displacement history normally obtained from tension or compression tests. The engineering stress-strain curve is converted to true stress-strain curve through simple formula. However, this procedure is valid only up to the onset of bulging where the state of stress becomes triaxial and the curve should be corrected to take account of this stress triaxiality. The correction of stress-strain curves after bulging has been the subject of many investigations over the past decades. Some of the methods are complicated and not applicable in practice.

Many researchers have studied different methods to obtain mechanical properties of different materials. It is very important to understand that the main approach to identify the compressive flow stress behavior is based on geometry changes during deformation.

In order to employ more advanced modeling tech-

niques, such as finite element analysis, the constitutive behavior at each point during the deformation regime must be determined.

Majzoobi et al. [1] proposed a new method for correction of true stress-strain curves in the tensile test after necking. This new method uses the surface strain of the specimen in the necking area which is measured by the image processing method. A new formula was proposed for correction factor using the plasticity theory in terms of the surface strain. Barati and Kazemi [2] obtained the flow stress-strain curves of AZ-71 magnesium alloy at high temperature and various strain rates and consequently the correction factor was obtained numerically. It seems that the first investigation was performed by Bridgeman [3] who presented a comprehensive analysis of stresses and strains in the necking area and proposed a correction factor (CF), based on the neck geometry, as follows:

$$CF = \left[\left(1 - \frac{2R}{a} \right) \ln \left(1 - \frac{a}{2R} \right) \right] \quad (1)$$

where R and a are the radius of the bulging curve and maximum barrel radius respectively. The radius R must be computed during the compression tests at regular time intervals. The correction factor is used as follows:

$$\sigma_e = Cf \cdot \sigma_{true} \quad (2)$$

where σ_e is equivalent or corrected stress. Existence of friction between the specimen end faces and the compression testing machine dies causes bulging (barreling) of the specimen that results 3D state of the stresses. Siebel and Pomp [4] proposed a correction factor formula in terms of the friction coefficient as follows:

$$C.F. = 1 + \frac{2\mu r(\varepsilon)}{3h(\varepsilon)} \quad (3)$$

where μ is the friction coefficient, r and h are the radius and height of the specimen in terms of the effective strain respectively. This method is one of the basic methods for correction of the compression stress-strain curve. In the extrapolation method proposed by Kocaker [5] specimens of different slenderness ratios are compressed. The “friction-free” flow curve is obtained by extrapolating the test results to $r_0/h_0 = 0$. Theoretically, for a cylinder of infinite length the end effects would be negligible; the barreling effect would therefore be absent and the mean compressive pressure could be taken as the true stress in axial compression. This method has been studied recently by Sato and Takeyama [6]. The advent of finite element method led to introduction of other methods for correction of stress-strain curves. Parteder and Bünten [7] proposed a new numerical method. Regarding the material flow data as experimental data, friction-free flow curve can be obtained even in the first iteration with enough accuracy. Parteder and Bünten [7] successfully applied this method to obtain flow curve from a compression test under sticking friction conditions and called this method as iterative finite element procedure. In this work it was assumed that strain rate dependency was negligible and isothermal conditions were satisfied; force-displacement curve was used to obtain force-plastic displacement curve from Fem. In this method error between the force from experimental and from the Fem method must be near the zero. Majzoubi et al. [8,9] corrected the stress-strain curve of the 304 stainless steel in compression test and determined the material parameters of the investigated material using finite element method; The barreling profile of the specimen was minimized from experiment and the numerical methods. In this method stress-strain curve was used as input of the numerical Fem program and output of the method was the profile of the barreling that must be similar to the experiment. Ettouney and Ehardt [10] introduced a new method that was derived from Bridgman’s correction factor but their method can be used in compression test.

2. Theory of the Method

Engineering stress-strain curve obtained from the load-displacement curve can be converted to the true stress-strain diagram through the following relations [1]:

$$\sigma_t = S(1 + e) \cdot \varepsilon_t = \ln(1 + e) \quad (4)$$

where e, ε_t, S and σ_t denote engineering strain, true strain, engineering stress, and true stress respectively. Eq. (4) holds only up to the point of bulging onset beyond which it is not usable. From image processing technique the diameter of the bulge section of specimen, d_p , and specimen’s elongation and height h_f , can be measured. After bulging, the cross-section areas will

not be constant. Therefore, true stress can be written as follows:

$$\sigma_t = \frac{P}{A_b} \quad (5)$$

where A_b is the maximum cross-section area of the maximum barrel radius. After bulging, the strain distribution is not uniform across the maximum barrel radius and varies in the longitudinal sections. With the uniform strain distribution assumption on the maximum barrel radius, strain can be computed taking account of the volume constancy assumption in plasticity which can be written from Fig. 1 as:

$$A_0 L_0 = A_b L_b \quad (6)$$

True or plastic strain can be written as follows:

$$\varepsilon_z = \ln L_0 = \ln A_b = 2 \ln \frac{r_0}{r_b} \quad (7)$$

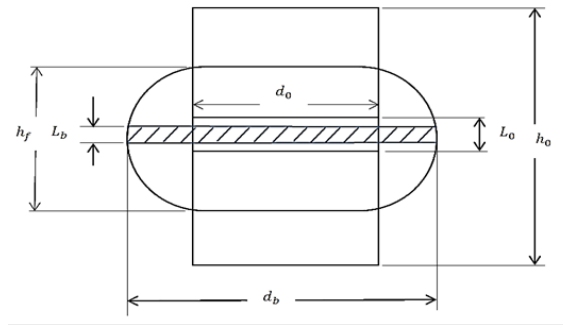


Fig. 1. Specimen geometry in the initial and the bulging condition.

The stress-strain curve obtained using Eqs. (5) and (7) must be corrected after the point of bulging. As a matter of fact, stress triaxiality at the bulging area necessitates the stress-strain diagram to be corrected. Effective stress and strain in the cylindrical coordinate based on principal stresses and strains are given by [1]:

$$\sigma_e = \frac{1}{\sqrt{2}} [(\sigma_z - \sigma_r)^2 + (\sigma_z - \sigma_\theta)^2 + (\sigma_\theta - \sigma_r)^2]^{1/2} \quad (8)$$

$$d\varepsilon_e = \frac{\sqrt{2}}{3} [(d\varepsilon_z - d\varepsilon_r)^2 + (d\varepsilon_z - d\varepsilon_\theta)^2 + (d\varepsilon_\theta - d\varepsilon_r)^2]^{1/2} \quad (9)$$

where z, r and θ are longitudinal, radial, and tangential directions respectively. The condition of volume constancy in the plastic deformation is defined as:

$$d\varepsilon_z + d\varepsilon_r + d\varepsilon_\theta = 0 \quad (10)$$

For a circular specimen in the tensile and compression tests, we can write [1,3]:

$$d\varepsilon_r = d\varepsilon_\theta \quad (11)$$

Substituting Eq. (11) in Eq. (10), the following equation is resulted:

$$d\varepsilon_r = d\varepsilon_\theta = -0.5d\varepsilon_z \quad (12)$$

In other words, the strain value in the radial and tangential directions are identical and are equal to minus of twice of the longitudinal strain. As seen before, the friction causes bulging of the specimen in the compression test and generation of a triaxial stress state in the barrel-shaped specimen. In this case equivalent stress-strain curve is used as the flow curve. Strain on the surface of specimen can be measured using image processing technique. In this technique, the initial and final distances between two points denoted by a_0 and a_f , respectively and marked by painted dots on the specimen (see Fig. 2) are measured.

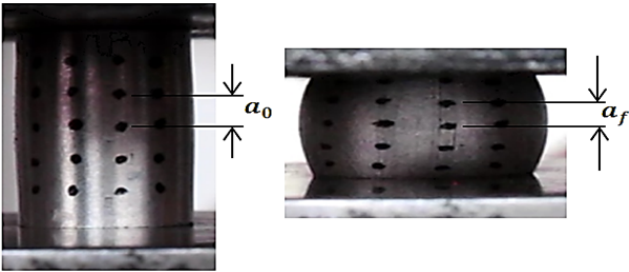


Fig. 2. Schematic representation of sandwich panel with corrugated core.

a_0 shows the distance between two marks before deformation and a_f is the final distance between the same points after deformation. These two quantities are used for calculation of the strain at a point. The strain at each point on the surface of the specimen is then obtained as follows:

$$\varepsilon_{sur,z} = \ln\left(\frac{a_f}{a_0}\right) \quad (13)$$

When the axial strain on the surface of specimen in the maximum barrel radius ($\varepsilon_{sur,z}$) is calculated from Eq. (13), the other two strain components, ε_r and ε_θ can be computed from Eq. (12). Therefore, in the proposed method, strain in bulging area in the z direction on surface of specimen is measured ($\varepsilon_{sur,z}$) by experiment. It must be noted that in contrast to Bridgeman [3] theory, strain distribution in maximum barrel radius is not uniform. In this study the strain distribution on the maximum barrel radius was considered as a function of the radius as $\varepsilon_{b,z}(r)$. In this method the specimen's bulging region is divided into n thin walled toroidal elements longitudinally as illustrated in Fig. 3.

In this figure, d_b and d_u denote the diameters of the specimen at the bulging and at the end point of the specimen, where deformation and consequently strain and stress are uniformly distributed. This area

is named as the uniform area. r_u^e and r_b^e denote the average radius of the element at the uniform and bulging areas respectively. The thickness of the element at the uniform and the bulging area are t_u^e and t_b^e respectively. The wall thickness of the elements t_u^e corresponding to d_u is the same for all elements and is obtained from the following relation:

$$t_u^e = \frac{d_u}{2n} = \frac{r_u}{n} \quad (14)$$

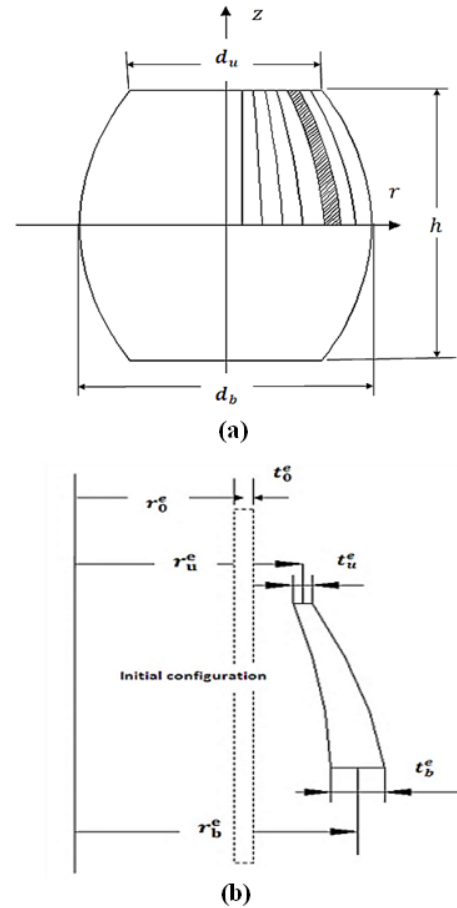


Fig. 3. (a) Some basic definitions on a bulged specimen, (b) Typical element.

However, this is not the case for the thickness of elements in the bulging zone. Therefore, the thickness of elements at this section (t_b^e) is not the same for all elements. Here, strain definition in r direction in maximum barrel radius section in the element “e” is used as follows:

$$\ln\left(\frac{t_b^e}{t_0^e}\right) = \varepsilon_{b,r}(r = r_b^e) = -0.5\varepsilon_{b,z}(r = r_b^e) \quad (15)$$

where $\varepsilon_{b,r}$, $\varepsilon_{b,\theta}$ and $\varepsilon_{b,z}$ are the radial, tangential, and longitudinal components of the strain on the maximum barrel radius for considered element respectively. Moreover, r_b^e is the average radius of element “e” in the maximum barrel radius, and t_0 is the initial thickness

of element and is equal to $t_0 = \frac{r_0}{n}$, and is the element thickness in the bulging area after deformation.

Now, consider an element as indicated in Fig. 4. The longitudinal stress and force acting on both ends of the element are shown in the figure. In the proposed model, the stress in the bulging zone of this element is calculated using the force equilibrium condition, $P_u^e = P_b^e = P^e$. Note that due to low thickness of elements, the radial stresses acting on the inner and outer surfaces of the element are equal to each other and are cancelled out from the equilibrium equation. The uniformly distributed longitudinal stress at the uniform distribution zone, which is shown in Fig. 13a, can be obtained from:

$$\sigma - u = \sigma_u^e = \frac{P}{\pi r_u^2} \quad (16)$$

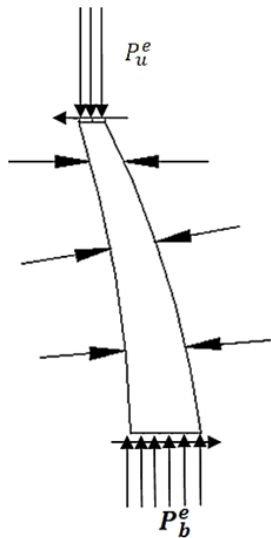


Fig. 4. Force free body diagram of the element.

where P is the compression force acting on specimen and can be determined from the force-displacement diagram obtained from the compression test. The longitudinal stress at the uniform zone was considered to have uniform distribution, which is one of the assumptions of the method. This consideration has approximately percentage error of 17%. Furthermore, σ_u and σ_u^e are the stress in the uniform cross-section and the stress in the element cross-section at the uniform zone respectively. Because of uniform deformation in this zone, stress values in the both sections are equal. Thus, it can be written as:

$$P_u^e = \sigma_u A_u^e = \frac{P}{\pi r_u^2} A_u^e \quad (17)$$

where P_u^e is axial load acting at the beginning of the bulging area, where deformation is uniform. From force equilibrium condition for element, as stated above,

force and stress in that element at the maximum barrel radius can be computed as:

$$P_b^e = P_u^e = P^e \quad (18)$$

$$\sigma_u A_u^e = \frac{P}{\pi r_u^2} A_u^e = \sigma_{b,z}^e A_b^e \quad (19)$$

where A_b^e and A_u^e are cross-sectional areas of the element in the maximum barrel radius and at the uniform section respectively. $\sigma_{b,z}^e$ is the longitudinal (z -direction) component of the stress in the maximum barrel radius. It can be written as:

$$A_b^e = 2\pi r_b^e t_b^e, \quad A_u^e = 2\pi r_u^e t_u^e \quad (20)$$

From Eq. (19) the longitudinal stress in the element "e" at the bulging zone ($\sigma_{b,z}^e$) can be written as:

$$\sigma_{b,z}^e = \left(\frac{P}{\pi r_u^2} \right) \left(\frac{A_u^e}{A_b^e} \right) \quad (21)$$

By substituting Eq. (20) in Eq. (21), the following equation can be derived as:

$$\sigma_{b,z}^e = \frac{2\pi P t_u^e r_u^e}{\pi r_u^2 2\pi r_b^e t_b^e} = \left(\frac{P}{\pi r_u^2} \right) \left(\frac{r_u^e}{r_b^e} \right) \frac{t_u^e}{t_b^e} \quad (22)$$

From Eq. (16) it can be written:

$$t_b^e = t_0 e^{\varepsilon_{b,r}(r=r_b^e)} = \frac{r_0}{n} e^{\varepsilon_{b,r}(r=r_b^e)} \quad (23)$$

By substituting Eqs. (23) and (14) in Eq. (22), Eq. (24) will be:

$$\sigma_{b,z}^e = \left(\frac{P}{\pi r_u^2} \right) \left(\frac{r_u^e}{r_b^e} \right) \left(\frac{\frac{r_u}{r_0}}{\frac{r_b}{n}} \right) e^{-\varepsilon_{b,r}(r=r_b^e)} \quad (24)$$

This equation gives z -component of stress in the element "e". However, it must be noted that from Eq. (8) this stress component in the outer element will be equal to the corrected or equivalent stress. The reason is that in this element the other two stresses ($\sigma_r^e - \sigma_z^e = \sigma_\theta^e - \sigma_z^e$) and $\sigma_r^e = 0$. Also from axisymmetric condition of the specimen equality of the radial and tangential components of strain and related stress were derived using analytical method. Also, for the outer element it can be written:

$$r^e = r_u, \quad r_b^e = r_b \quad (25)$$

By substituting Eq. (25) in Eq. (24), and from the Eq. (10) the following equation can be obtained:

$$\sigma_e = \left(\frac{P}{\pi r_b r_0} \right) e^{0.5\varepsilon_{sur,z}} \quad (26)$$

where $\varepsilon_{sur,z}$ is the longitudinal surface strain on the bulging area that can be measured from image processing method. By multiplying the numerator and

denominator of the right hand side of Eq. (26) by the following equation can be obtained:

$$\sigma_e = \left(\frac{P}{\pi r_b r_0} \right) \left(\frac{r_b}{r_0} \right) e^{0.5 \varepsilon_{sur,z}} = (CF) \sigma_{true} \quad (27)$$

where $\sigma_{true} = \frac{P}{\pi r_b^2}$ is the true or uncorrected stress and CF, so the correction factor is defined by:

$$CF = \left(\frac{r_b}{r_0} \right) e^{\varepsilon_{sur,z}/2} \quad (28)$$

Strain can be computed as:

$$\frac{r_b}{r_0} = e^{-\varepsilon_z/2} = e^{-0.5 \varepsilon_e} \quad (29)$$

By substituting $\frac{r_b}{r_0}$ from Eq. (29) in Eq. (28), Eq. (30) can be obtained as:

$$CF = e^{(\varepsilon_{sur,z} - \varepsilon_e)/2} \quad (30)$$

Thus, the correction factor of round specimen is expressed as a function of surface strain (in bulging area), which was obtained from image data in a compression test. Eq. (29) defines the stress-strain curve before and after bulging. Before bulging, strain is uniform and Eq. (29) can be written as:

$$\varepsilon_{z,s} = \varepsilon_z = \varepsilon_e \quad (31)$$

In this case, we have $CF = 1$ and Eq. (29) is reduced to:

$$\sigma_e = \sigma_{true} = \frac{P}{A} \cdot CF = e^{(\varepsilon_{sur,z} - \varepsilon_e)/2} \quad (32)$$

3. Compression Test and Strain Measurement

Compression tests were conducted on a universal testing machine (60-ton Instron model 8503). Specimens were made of the steel St 304 according to the standard ASTM-E9 [11]. The specimens shown in Fig. 5 had a length of 30mm and a diameter of 20mm. The compression tests were conducted at rate of 5mm/min at ambient temperature. A Handycam (DCR-HC32E model) with 30fps and 800KP resolution was employed to record the deformation of the specimens. From the captured images, the diameter and the profile of the specimen in the bulging area were measured. This was accomplished using the images captured by camera as shown in Fig. 6. In order to measure the profile of the specimen at a specific time, the image of the specimen which was captured by camera during compression test was selected at that time. Then using Digitizeit and Getdata software, the geometrical information such as the length of the specimen, diameter, and profile were measured.

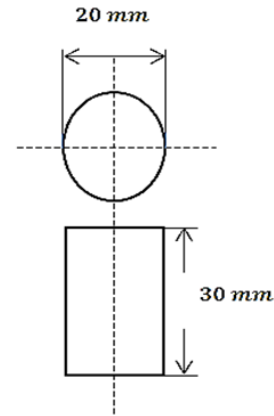


Fig. 5. The specimen dimensions.

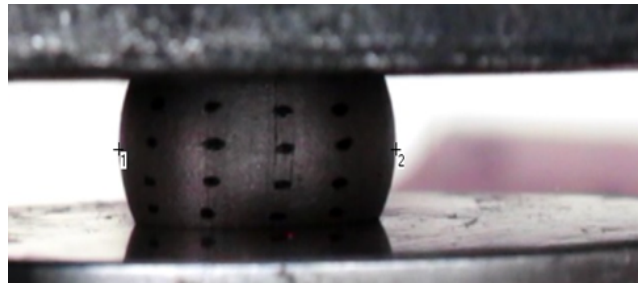


Fig. 6. The digital approach for measuring the profile of specimen.

The load-displacement, the engineering stress-strain curve, and the true stress-strain curve of the specimen are shown in the Figs. 7, 8 and 9 respectively.

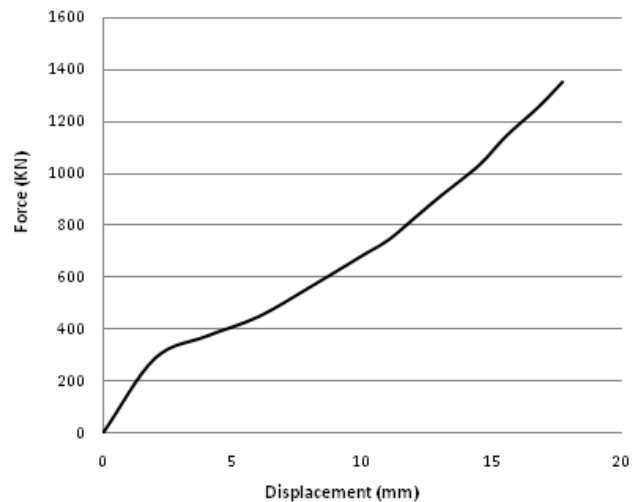


Fig. 7. The load-displacement curve of the compression test.

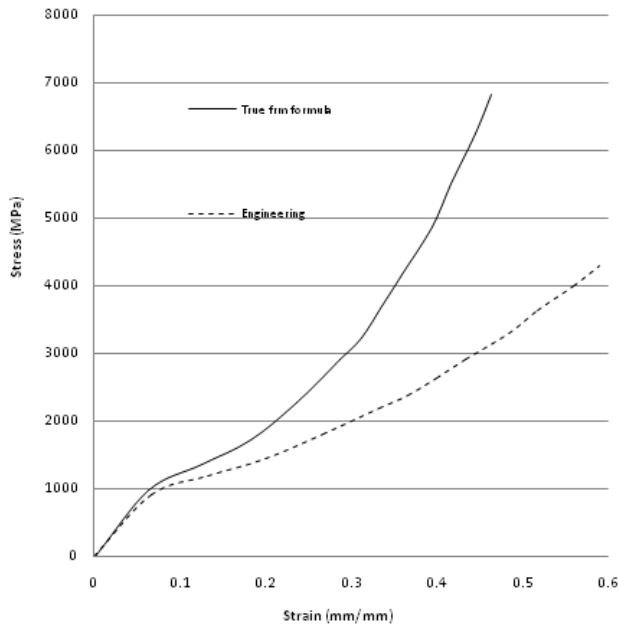


Fig. 8. Engineering stress-strain curve and True stress-strain curve obtained using Eq. (4).

The engineering stress-strain curve and the true stress-strain diagram obtained using Eq. (4) are illustrated in the Fig. 8. The true stress-strain curve extracted from image processing, experimental data, and use of the Eqs. (5) and (7) are illustrated in Fig. 9. In the Fig. 8 a power law is assumed for the stress-strain curve; from a curve fitting to the true stress-strain curve, the following piecewise function can be obtained easily:

$$\sigma = K\varepsilon^n, \quad K = 1551.5, \quad n = 0.294 \quad (33)$$

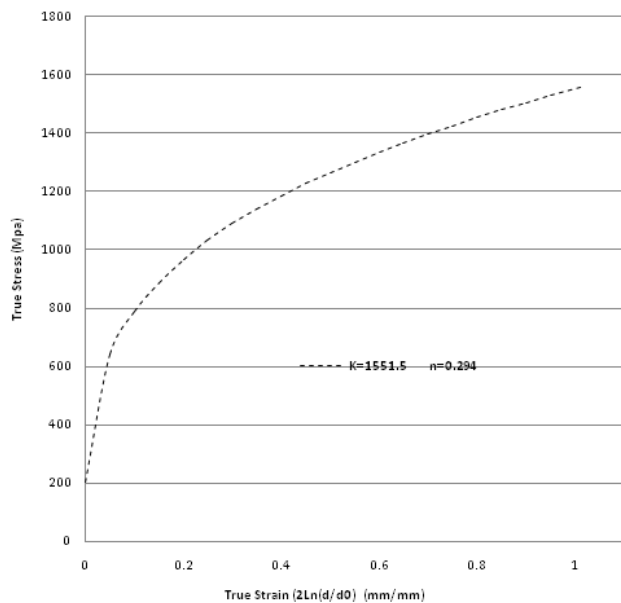


Fig. 9. True stress-strain curve obtained from image measurement of the diameter of the bulging section.

The true stress-strain shown in Fig. 9 is not usable after bulging and should be corrected taking effect of the stress triaxiality. The strain on the bulging surface of the specimen in compression test was measured using the images shown in Fig. 2. As it is seen in Fig. 2, the points are printed on the specimen randomly. The strain history of each point can be obtained through the procedure explained in the manuscript. Table 1 shows the surface strain-time history of one of these points on the bulging surface. The details of the surface strain measurement are shown in the Fig. 2, where the distances between two points before and after deformation are illustrated. The displacement between the points was used to compute the surface strain at that point. The points were tried to be selected close to the maximum barrel radius as much as possible.

Variation of z-strain versus time is illustrated in Fig. 10. The equal number of points shown in Fig. 10 can be used to obtain the corrected true stress-strain curve; desired number of points can be also used in time interval. The corrected stress is calculated at the sample points. The points are then fitted into a curve.

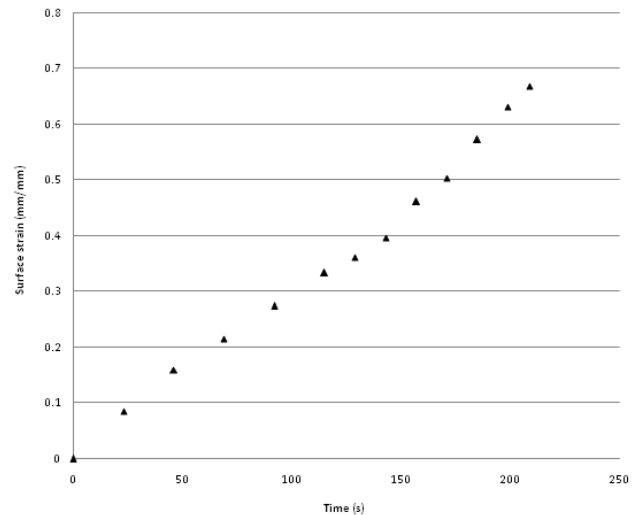


Fig. 10. The variation of z-strain versus time on the bulging surface measured by the image processing.

The procedure of calculating the corrected stress from the proposed method can be summarized as follows:

1. Measure $\varepsilon_{sur,z}$ from image data at sample times.
2. Calculate $\varepsilon_z = 2 \ln \frac{r_0}{r_b}$ at sample times.
3. Calculate correction factor (CF) or σ_e using Eq. (30) at the sample time.
4. Repeat steps (1) to (3) for the times $t_1 + m\Delta T$, where $1 \leq m$ and m is arbitrary.

A comparison between the uncorrected stress-strain curve obtained using experimental data and its corre-

sponding corrected curve using the data given in Table 1 is shown in Fig. 11.

Table 1

Surface strain, average strain and the correction factor at different times on bulging section.

t	$\varepsilon_{sur,z}$	ε_e	CF	t	$\varepsilon_{sur,z}$	ε_e	CF
0	0.00	0.00	1.000	143	0.4	0.65	0.880
23	0.09	0.11	0.988	157	0.46	0.72	0.880
46	0.16	0.22	0.973	171	0.50	0.81	0.858
69	0.22	0.3	0.961	185	0.57	0.89	0.855
92	0.27	0.40	0.939	199	0.63	0.96	0.847
115	0.33	0.52	0.912	209	0.70	1.03	0.837
129	0.36	0.58	0.898				

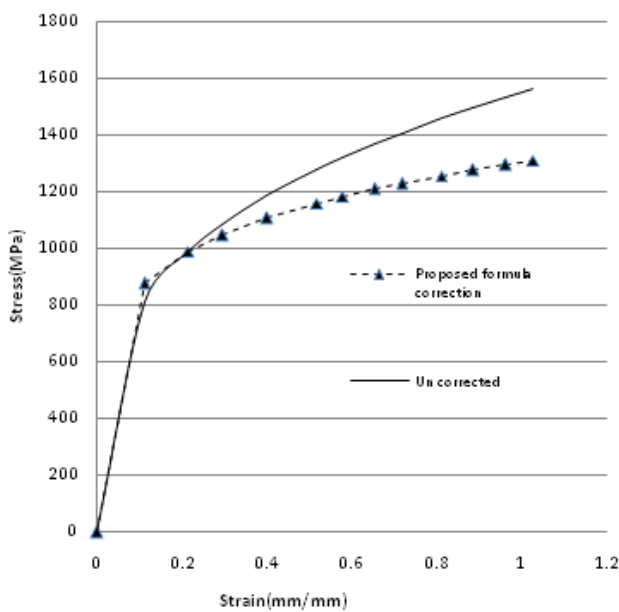


Fig. 11. A comparison between the uncorrected stress-strain curve obtained using experimental data and its corresponding corrected curve using the data given in Table 1. Better to correct the title.

4. Numerical Simulation and Optimization

In order to obtain the constants of constitutive material model, measures were taken to minimize the differences between the numerical predictions of specimen's deformation and those obtained from the experiments. The differences were taken as the objective function of an optimization problem. The constants of the constitutive model were adopted as the variables of the problem. The objective function was defined by a polynomial given by the Eq. (7):

$$OBJ(x) \approx a_0 + \sum_{i=1}^n a_i v_i + \sum_{i=1}^n b_{ij} v_i v_j \quad (34)$$

where $v_i (i = 1 - n)$ is the vector of the constants; the coefficients a_i and b_{ij} are determined from the numerical simulations and n is the number of constants of the material model under investigation. The number of coefficients a_i which needs to be obtained from the simulation solution of a system of n algebraic equations specifies the number of numerical simulations required for each compressive test. This is achieved by considering n different sets of constants for the material model for the simulation of each test. The genetic algorithm was employed to find the optimums of n, k and μ . In this study, the optimum constants were obtained from the numerical simulations of compressive tests. The optimization is summarized in Table 2.

Table 2

Surface strain, average strain and the correction factor at different times on bulging section.

Material model	Number of variables	Number of simulation	Optimization variables
power-law	3	13	n, k, μ

As stated above, the objective function is defined as the difference between the deformed shapes predicted from simulation and measured from the experiments. The three variables, including the initial and the barrel maximum diameters and the height of the bulged specimen were designated for the optimization process as illustrated in Fig. 12. These variables were measured by experiment using the image processing technique. The objective function is defined as follows:

$$OBJ = \sqrt{(d_{1e} - d_{1n})^2 + (d_{2e} - d_{2n})^2 + (h_e - h_n)^2} \quad (35)$$

where d_{1e} is the maximum diameter in the middle of the specimen, d_{2e} is diameter on the initial surface, and h_e is the height of specimen after deformation that all of them are measured by using image processing technique from test specimen as shown in Fig. 12. Also, d_{1e} , d_{2e} and d_{3n} are the maximum diameter in the middle of the specimen, diameter on the initial surface, and the height of specimen that all of them were computed from numerical and modeling method.

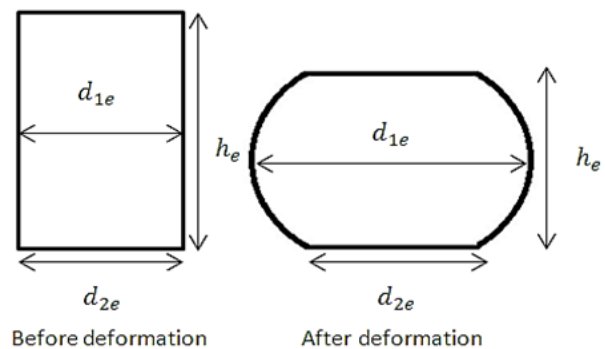


Fig. 12. Designated diameters and heights on the bulging area for optimization purpose.

Alternatively, the objective function is defined by [7]:

$$OBJ(n, k, \mu) = a_0 + a_1n + a_2k + a_3\mu + a_4nk + a_5n\mu + a_6k\mu + a_7n^2 + a_8k^2 + a_9\mu^2 + n^2k^2a_{10} + a_{11}n^2\mu^2 + a_{12}k^2\mu^2 \quad (36)$$

Numerical simulation was done using ABAQUS finite element software. The geometry was axisymmetric and the axisymmetric elements were used, so just half of the specimen was considered for numerical modeling. The model consisted of 3300 elements type of CAX4R, which are four-noded axisymmetric bilinear quadrilateral elements. All the nodes at the bottom of the cylinder were not allowed to move in the z direction because of the rigid plate, which was not allowed to move whereas all the nodes at the top of the cylinder were allowed to move in the z direction. Fig. 13 shows the meshing, boundary conditions, and a typical deformation after bulging. The material characteristics include Young's modulus $E=210\text{GPa}$, Poisson's ratio $\nu = 0.3$, and the corrected stress-strain curve for stainless steel 304L. In the end with doing 13 simulations with different sets of n, k and μ and solving a system of 13 algebraic equations, the coefficient of the Eq. (36) was obtained (see Table 4). Thirteen different sets of n, k and μ with their corresponding diameters from simulation were calculated.

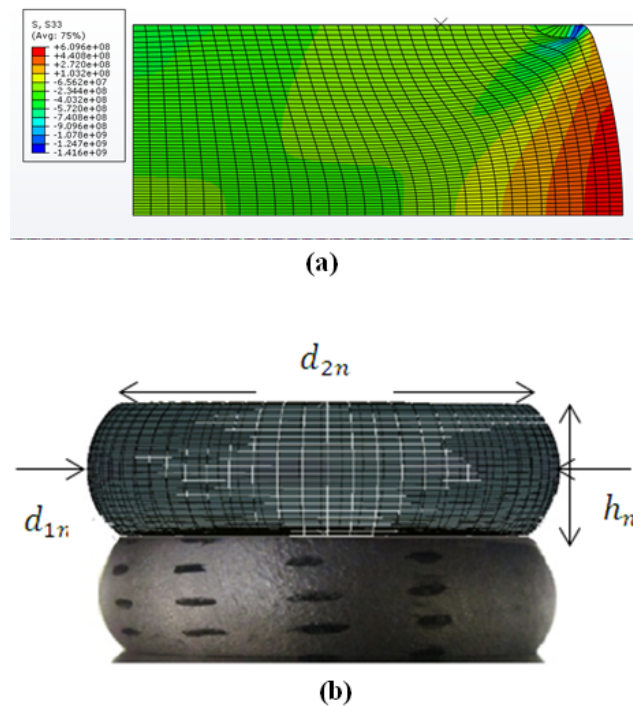


Fig. 13. (a) Finite element longitudinal stress distribution, (b) a typical deformation.

Table 3
Constants in equation (36).

Value	Coefficients
a_0	2142.551357
a_1	-11216.17987
a_2	-5.041960061
a_3	54701.65712
a_4	11.87130737
a_5	20996.04814
a_6	-35.21613213
a_7	-4539.242014
a_8	0.002259449006
a_9	-1.504534315×10^5
a_{10}	-0.009969096055
a_{11}	8.766904685×10^5
a_{12}	0.02762109818

Table 4
The values of (n, k, μ) .

n	k	μ
0.207764376849066	1300	0.08

The load-displacement curves from test and the numerical methods with modeling is shown in Fig. (14).

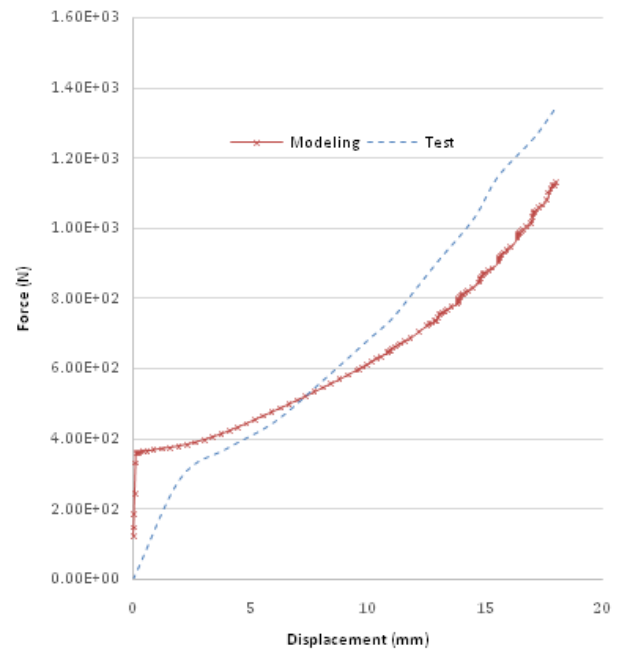


Fig. 14. The load-displacement curves from test and the numerical methods.

5. Validation of the Method and Discussion

Bearing in mind that the material model used in the numerical simulations is the same as the corrected stress-strain curve, it can be argued that this curve obtained from the optimization-aided numerical simulations is the most accurate one. The first reason is that the numer-

ical simulations provide the minimum difference between the numerical and experimental bulge profiles. As a matter of fact, it is argued that the numerical and experimental bulge profiles cannot coincide unless a correct stress-strain curve (or a proper material model) is used in the simulations.

The second reason is that the numerical simulations are free of measurement errors which occur during the image processing and the tests. Therefore, the numerical results were considered as a benchmark for evaluating the accuracy of the other methods for obtaining the correction factor. Therefore, numerical simulation was used for validation of the proposed method. For this purpose, the constants K and n were computed through simulation of compression test and the bulging. In this approach, K and n are determined in a way that the experimental and numerical profiles of the barreling are coincident. Genetic algorithm was employed to minimize the difference between the two profiles. A genetic algorithm (GA) is an optimization technique inspired by natural evolution such as inheritance, mutation, selection, and crossover. Fig. 15 shows the results of the proposed method with the numerical optimization methods together. Although, the value of the material parameter from the different methods is shown in Table 5.

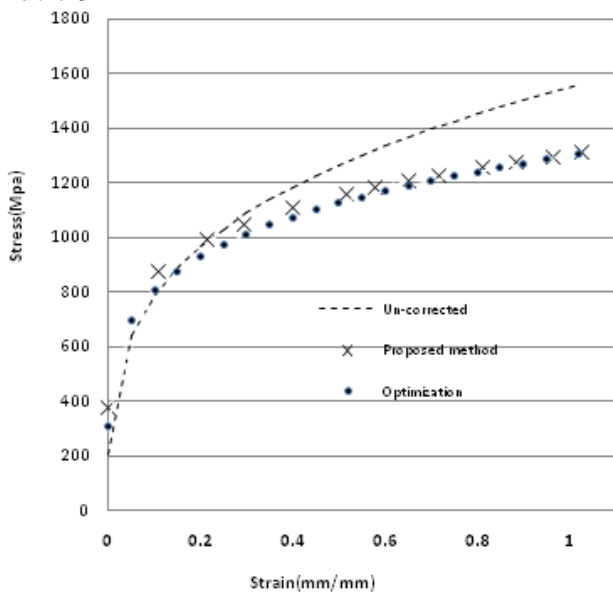


Fig. 15. A comparison between the uncorrected true stress-strain and the corrected curves obtained using the proposed method and optimization method.

A genetic algorithm (GA) is a method for solving both constrained and unconstrained optimization problems based on a natural selection process, which mimics biological evolution. The algorithm repeatedly modifies a population of individual solutions. At each step, the genetic algorithm randomly selects individuals from the current population and uses them as parents to produce the children for the next generation.

Over successive generations, the population evolves toward an optimal solution. The genetic algorithm can be applied to solve problems that are not well suited for standard optimization algorithms, including problems in which the objective function is discontinuous, non-differentiable, stochastic, or highly nonlinear.

Table 5

The values of K and n corresponding to the Un-corrected, proposed and the optimization methods.

Method	K	n
Un-corrected	1551.53	0.3
Proposed formula	1305.05	0.18
Optimization	1300	0.21

6. Conclusions

The values of K and n obtained using proposed method and optimization are provided in Table 5 and their corresponding corrected stress-strain curves are shown in Fig. 14. It might be argued that optimization aided numerical simulations with providing the most accurate prediction because they provide the best agreement with the experiment on the bulging profile. The corrected stress-strain curves from proposed formula and the corrected curve from optimization method that is shown in the Fig. 14, shows that the proposed formula can be used as the applicable method for correction purpose. Furthermore, in this formula the correction factor is in terms of the surface strain on bulging area that is determined more simple and accurate than curvature radius that is used in the Bridgeman method.

From the results obtained in this investigation, the following conclusions may be drawn:

1. The proposed correction method can be trusted for correction of stress-strain curves. The reasons: (i) it is derived based on plasticity and requires only a few experimental measurements which can be easily performed, (ii) it provides the best agreement with numerical simulation.
2. The proposed correction factor formula is in terms of the surface strain whereas most of other models are based on bulging curvature such as Bridgeman.

References

- [1] G.H. Majzoobi, F. Fariba, M.K. Pipelzadeh, S. Hardy, A new approach for the correction of the stress-strain curves after necking in metals, *J. Strain. Analysis.*, 13 (2014) 253-266.
- [2] F. Barati, S. Kazemi, Modeling flow stress compressive curves of AZ71 Magnesium alloy at high temperature and various strain rates, *J. Science and Today World.*, 3 (2014) 72-74.

- [3] P.W. Bridgeman, The stress distribution at the neck of a tension specimen, *Trans. Amer. Soc. Metal*, 32 (1944) 553-574.
- [4] E. Siebel, A. Pomp, Determination of flow stress and friction with the upsetting test. *Mitt. KWI*, 9 (1927) 157-171.
- [5] Kocaker, B, Production properties prediction after forming process sequence, MSc Thesis. Turkey: Middle East Technical University; 2003.
- [6] Y. Sato, Y. Takeyama, An extrapolation method for obtaining stress-strain curves at high rates of strain in uniaxial compression, *Tech. Rep. Tohoku Univ.*, 44 (1980), 287-302.
- [7] E. Parteder, R. Bünten, Determination of flow curve by means of a compression test under sticking friction condition using an iterative finite- element procedure, *J. Mater. Process. Tech.*, 74 (1998) 227-223.
- [8] G.H. Majzoobi, F. Fres, Determination of material parameter under dynamic loading part I: Experiments and simulation, *J. Comp. Mater.*, 49 (2010) 192-200.
- [9] G.H. Majzoobi, R. Bagheri, J. Payandeh-Peyman, Determination of material parameter under dynamic loading part II, Optimization, *J. Comp. Mater. Sci.*, 49 (2010) 201-208.
- [10] O. Ettetouny, D. Ehardt, A method for in-process failure prediction in cold upset firing, *J of engineering and industrial*, 105 (1983) 161-167.
- [11] ASTM, E8. Standard methods of tension testing of metallic materials, Annual book of ASTM standard. American society for testing and materials. 3.01.